ISSN 1862-6300
Phys. Status Solidi A
208 · No. 6 June
1209–1480 (2011)

physica status solidi a

www.pss-a.com

applications and materials science

6
2011

Ordered silicon nanopillars and nanowires by self-assembly and metal assisted etching

Luca Boarino, Dario Imbraguglio, Emanuele Enrico, Natascia De Leo, Federica Celegato, Paola Tiberto, Nicola Pugno, and Giampiero Amato

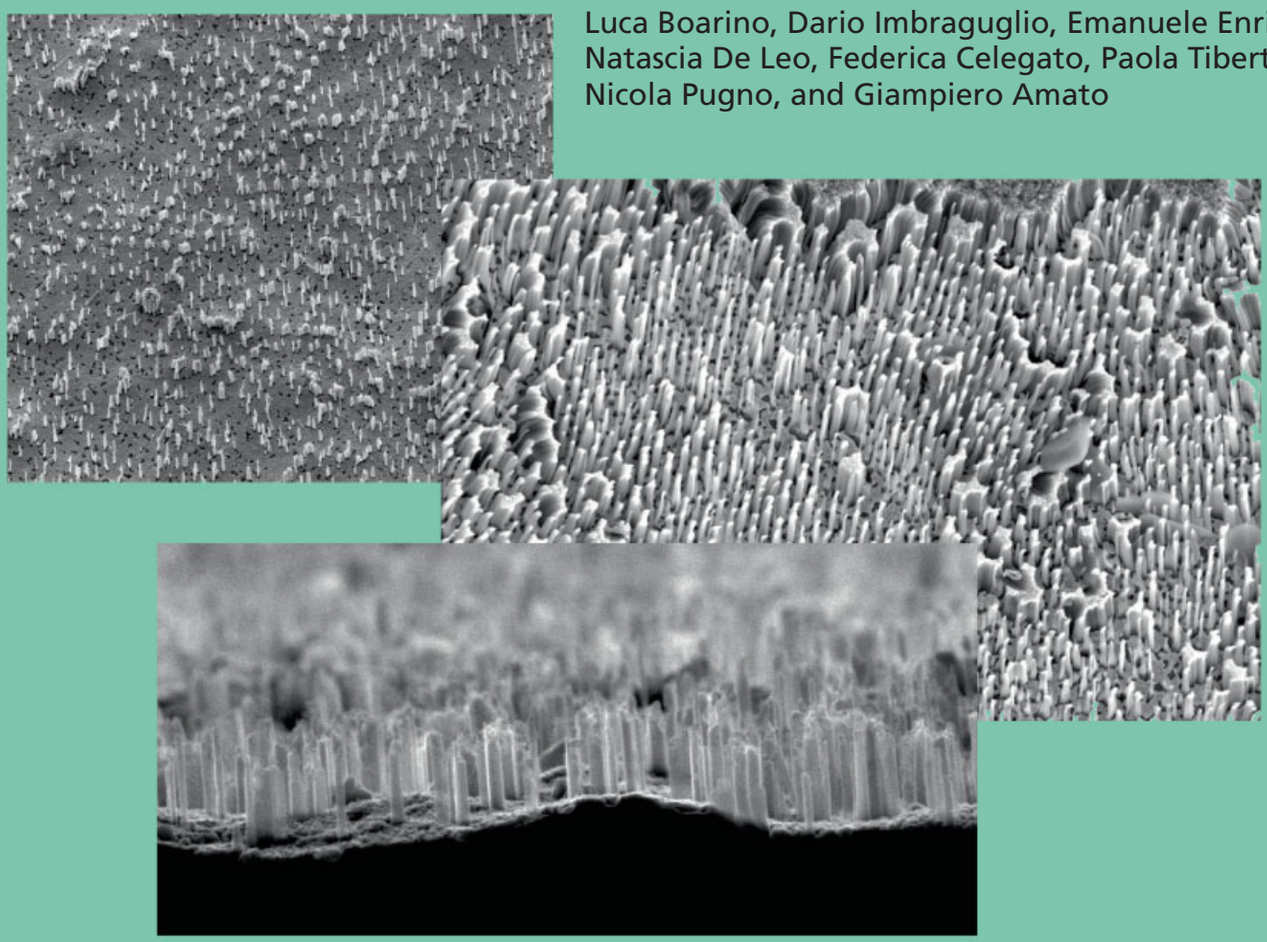

WILEY-VCH

50 years physica status solidi pss 1961–2011

physica status solidi a
208 · 6 · June 2011

Phys. Status Solidi A **208**, No. 6, 1412–1416 (2011) / **DOI** 10.1002/pssa.201000182

physica status solidi a
www.pss-a.com
applications and materials science

Fabrication of ordered silicon nanopillars and nanowires by self-assembly and metal-assisted etching

Luca Boarino*[,1], Dario Imbraguglio[1], Emanuele Enrico[1], Natascia De Leo[1], Federica Celegato[1], Paola Tiberto[1], Nicola Pugno[2], and Giampiero Amato[1]

[1] NanoFacility Piemonte, Electromagnetism Division, Istituto Nazionale di Ricerca Metrologica, Strada delle Cacce 91, 10135 Turin, Italy
[2] Laboratory of Bio-inspired Nanomechanics "Giuseppe Maria Pugno", Department of Structural and Geotechnical Engineering, Politecnico di Torino, C.so Duca degli Abruzzi 24, 10129 Turin, Italy

Received 29 April 2010, revised 30 October 2010, accepted 24 November 2010
Published online 18 March 2011

Keywords metal-assisted etching, nanopillars, nanowires, self-assembly, silicon

* Corresponding author: e-mail l.boarino@inrim.it, Phone: +39 11 3919343, Fax: +39 11 346384

Silicon nanowires (SiNWs) and nanopillars have been obtained by metal-assisted etching (MAE), starting from silver thin films deposited by thermal evaporation and sputtering on silicon substrates. Different deposition methods and thickness are strongly affecting spatial distribution and shapes of the extruded silicon nanostructures. The paper reports a study of distribution and morphology, as a function of silver thickness, deposition conditions and etching times. The application of polystyrene soft masks obtained by self-assembly and the sputter-etching by Ar ions allow the formation of regular indentations in the silver thin films, giving origin to a regular distribution of extruded pillars and wires during the following etching in HF:H_2O_2:H_2O. The aqueous etching and the use of silver still influence the homogeneity of the etching result on large area and introduce a modulation in the etching front, so affecting thickness homogeneity. Work is in progress to replicate these former results with gold and different etching solutions.

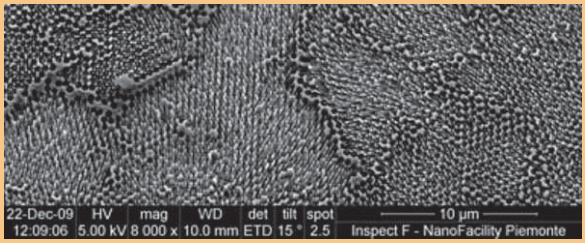

SEM microphoto of ordered SiNWs obtained by MAE and polystyrene nanosphere self-assembly.

1 Introduction The field of silicon nanowires (SiNWs) saw, in the last years, a real boom in the number and quality of publications. A part the basic research, investigating fundamental properties like electron transport [1] and mechanics [2], several fields of application can take advantage from SiNWs, like photovoltaic energy production by means of new generation devices [3], energy harvesting by vibrations [4] and new adhesives [5].

The recent development of self-catalytic electroless etching in presence of metals [6], offers a new degree of freedom in nanofabrication, because this kind of etching is only slightly dependent on silicon wafer doping and from solutions and etching conditions [7] but mainly from metal distribution, thickness or patterning at the silicon surface. We used these different conditions, from continuous thin silver films deposited by different methods and with different thickness to obtain a nanopatterning of thin silver films by means of self-assembled monolayers of polystyrene nanospheres (PSNS). In this way it is possible to obtain forests of SiNWs with different spatial density, distribution and order.

2 Experimental results and discussion Silicon wafers by MEMC Corporation, ⟨100⟩ 20–30 Ω cm have been cleaned by RCA for 1 h to remove organic contamination, and then silver thin films of different thickness (20, 30

Figure 1 Processing steps for SiNWs and nanopillars fabrication by MAE and PSNS self-assembly.

and 40 nm) have been obtained by thermal evaporation or sputtering with typical conditions are of 50 W RF power and Ar^+ pressure of 10^{-2} mbar. SEM investigations have been performed by a FEI Inspect F to check thin film quality. Subsequently, a large 2D crystal of Sigma–Aldrich 500 nm PSNS has been self-assembled and carefully lifted on the substrate. After drying, sputter etching by Ar^+ ions is performed, with RF power of 100 W, Ar^+ pressure of 10^{-2} mbar and with times ranging from 1 to 3 min (processing steps sketched in Fig. 1), to obtain a silver film with regular indentation favouring the extrusion of silicon nanopillars and nanowires in the following etching step.

After sputter-etching, nanospheres have been removed by sonication in hot acetone or toluene. At this point metal-assisted etching (MAE) has then been performed for all the samples for with times ranging from 10 to 60 s at 60 °C in a solution of HF:H_2O_2:H_2O, 22%:9%:69% in volume.

2.1 Polystyrene nanospheres lithography PSNS are commonly utilised in phase separation processes. Recently these particles have been used to form self-assembled masks for nanolithography on large area [8–11].

In general, heterophase polymerizations [12] are the techniques of election for the preparation of these and other colloids, including a variety of different processes like suspension, dispersion, emulsion [13] as well as nanoemulsion polymerizations [14, 15].

Self-assembly is the natural alternative to top-down fabrication at the nanoscale. The top-down approach of semiconductor industry has severe limitations under the dimension of 100 nm, because optical lithography, the widest technology used to define in parallel geometries and patterns, is affected by diffraction problems under 500 nm for the UV light. Higher energy radiations and liquid immersion lithography can be used to push down the resolution to 190 nm, but often sequential methods, like Electron or Ion Beam Lithography, are adopted, leaving the application and design of small geometries at the nanoscale on a large areas unresolved.

Self-assembly is a parallel process where from a disordered system the order appears and is strictly related to the control of size, shape and surface properties of the building blocks, like charge, hydrophobicity and functionality. These properties manage the attractive and repulsive forces among the building blocks so being responsible for the self-assembly.

Energy minimization, without external influence, drives the self-assembly of building blocks to form structures in static equilibrium.

2.2 Formation of 2D arrays of colloidal spheres Monodispersions of nanospheres can be assembled in ordered 2D crystals and arrays on solids or thin films with several methods [16–19], the most common being on a liquid surface by attractive long-range interactions, in a thin film of liquid spread on a solid using attractive capillary forces or via electrophoretic deposition on the surface of a solid electrode.

We used the first method, forming the 2D crystal of spheres on the air–liquid interface and then lifting it on the surface of a solid substrate. The spreading on the water surface is rather critical, since the monodispersions of nanospheres are charged with surfactant groups (typ. SO_4^-) and a fast diffusion of the nanospheres occurs on the liquid. To counterbalance these repulsive forces, a spreading agent, typically alcohol, is added to the monodispersion, in 1:1 or 1:2 ratio. This allows a different floating level on the water surface to be reached, thus screening the repulsive contributes with dipoles induced by the molecules of liquid [20–22]. To facilitate the aggregation in a big crystal, even if composed of domains with different orientations, an anionic surfactant (sodium dodecil sulphate, 5 vol%) can be added at the water surface, repulsing and compacting the various floating crystals. With this method, a number of parameters like alcohol content, surface hydrophobicity, initial charge density on nanospheres and physico-chemical properties of the liquid and spreading conditions on the air–liquid surface are crucial for the self-assembly of large 2D floating crystals.

2.3 Sputter etching After self-assembly of nanospheres, and subsequent lifting on a silicon substrate and drying, the samples were sputter-etched at a power of 100 W and 10^{-2} mbar of Ar for 1 min. This etching works as a localized indentation of the silver layer, since the Ar^+ ions can reach the thin metal film only at the interstitial sites among the spheres, obtaining this way an array of nanoindentations in hcp geometry.

2.4 Metal-assisted etching MAE has been recently proposed by Bohn and coworker [23]. The preferred materials for this kind of etching are the noble metals like Au, Ag and Pt, but other metals can be in principle used, like Co and magnetic alloys, with the limitation of low etch rates due to the dissolution of these metals in HF.

MAE is a sort of self-catalytic etching of silicon and other semiconductors, with no need of polarization, differently from electrochemical etching. The formation mechanism is in fact ruled by local redox potential of the metal respect to silicon, driving the holes necessary to dissolution at the metal–semiconductor interface. Metals can be deposited in form of thin solid films, or by precipitation starting from liquid metallic salts like $AgNO_3$ and others.

The metal clusters at the surface of the silicon wafer, rapidly sink following the crystallographic directions, and define silicon walls or wires, depending on the metal particle distribution at surface, the sample temperature and the concentration of the etchants. In our case, since the metal

is patterned on the surface, MAE leads to regular morphologies.

The dissolution of silicon in HF and an oxidizing agent like hydrogen peroxide is a combination of chemical and electroless process, having strong similarities with porous silicon formation or electropolishing by stain etching in HF-HNO_3.

In electrochemical silicon etching, currents flow from anode to cathode sites, and the two or four holes are required for silicon atom removal, depending if the regime is porous silicon formation or electropolishing. In the case of MAE, holes are injected in silicon by H_2O_2, independently from the original substrate doping. In this case, the oxidizing agent concentration plays the role of current density in electrochemical processes. HF concentration rules dissolution and surface chemistry at the same way for both the processes. The ratio between oxidizing agent and HF deeply affects the etching regimes and the morphologies.

The silver clusters at the silicon surface are charged with electrons that, due to charge compensation, tend to localize holes at silicon–silver interface. The majority of these holes are produced by H_2O_2 dissociation at cathode in presence of catalyzing silver, as shown in Eq. (1) and forming SiO_2 or removing Si at anode, as in Eq. (2).

2.4.1 Cathodic reaction The Ag particles at the cathode, catalyze the reduction of H_2O_2 as in Eq. (1) taking advantage from a favourable redox potential, and enhancing the etch rates by supplying free holes in proximity of Si–Ag interface.

$$H_2O_2 + 2H+ \rightarrow 2H_2O + 2h + E0 = +1.76\,V/NHE. \quad (1)$$

2.4.2 Anodic reaction In analogy to the chemical dissolution of Si in HF–HNO_3 [24, 25] summarizing the different mechanisms proposed in the literature [26] and following the work of Chartier and coworkers [7], the anodic reaction is proposed as:

$$Si + 6HF + nh^+ \rightarrow H_2SiF_6 + nH^+ + \left[\frac{4-n}{2}\right] H_2. \quad (2)$$

The general form is valid for porous silicon formation and electropolishing, where n, ranging from 2 to 4, is the number of holes per dissolved Si atom.

In the case of $n = 2$, porous silicon formation occurs, with the following overall dissolution anodic reaction:

$$Si + 4HF_2^- \rightarrow SiF_6^{2-} + 2HF + H_2 + 2e^-.$$

$$E0 = -1.2\,V/NHE. \quad (3)$$

well below the critical current density of electropolishing (JPS) and also valid for HF/HNO_3 stain etching

In the case of $n = 3$, ½ H_2 per dissolved silicon atom, as in the case of 6 M HF – 6 M HNO_3 solutions [26] or in stable electrochemical dissolution at JPS [27].

The electropolishing regime occurs when $n = 4$, as for low HF/HNO_3 ratio or for current densities higher than JPS, with a different mechanism involving the formation and dissolution of intermediate species like SiO_2 and without H_2 formation (4a, 4b).

$$Si + 2H_2O \rightarrow SiO_2 + 4H^+ + 4e^- \; E0 = -0.84\,V/NHE. \quad (4a)$$

$$SiO_2 + 2HF_2^- + 2HF \rightarrow SiF_6^{2-} + 2H_2O. \quad (4b)$$

3 Discussion The morphologies resulting from MAE are deeply affected by the distribution of metal particles on the silicon surface, so the use of PSNS self-assembly and MAE is rather interesting for application fields requiring a large-area nanostructuration, like sensors, anti-reflection layers in photovoltaics, functional materials and surfaces. Recently, Gösele and coworkers [28] used a mask of self-assembled PSNS to grow ordered pillars and wires by means of MBE. Our method allows for higher aspect ratios, with more affordable equipment.

Figure 2 shows the extruded array of SiNWs resulting from 30 s of MAE. Ordered areas of nanowires with average diameter around 30 and 300 nm long are evident in the SEM micrograph (detail in Fig. 5).

The geometry of the wires is in general triangular or polygonal, determined by the shape of the silver area removed by the argon ion bombardment. Different silver thicknesses have been used, 20, 30 and 40 nm, the best results outcome from the 30 nm thin films. In the case of 20 nm and less, in fact, undesired wires are forming among the metal grains of silver, and with 40 nm the metal layer tends to delaminate during etching in HF:H_2O_2. The ideal thickness obviously depends on the quality of the deposition method.

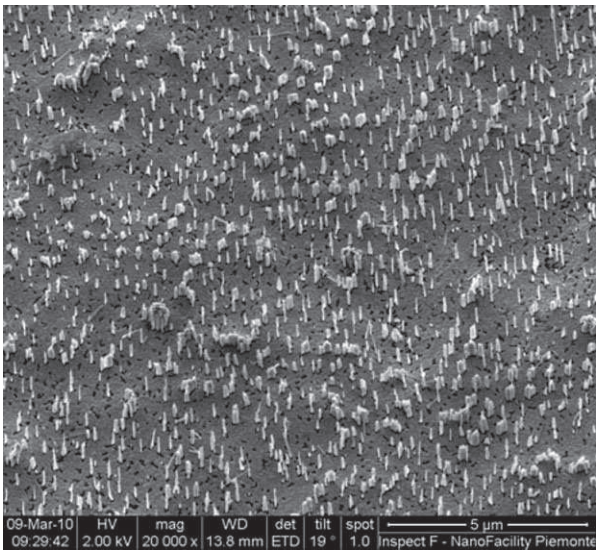

Figure 2 Ordered areas of SiNWs obtained through the process described in Fig. 1.

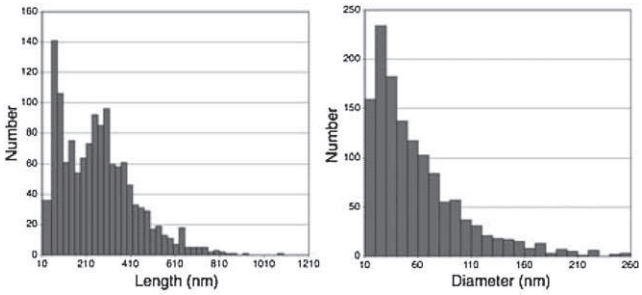

Figure 3 Distribution of nanowire lengths and diameters along the array, as calculated by means of morphological analysis software.

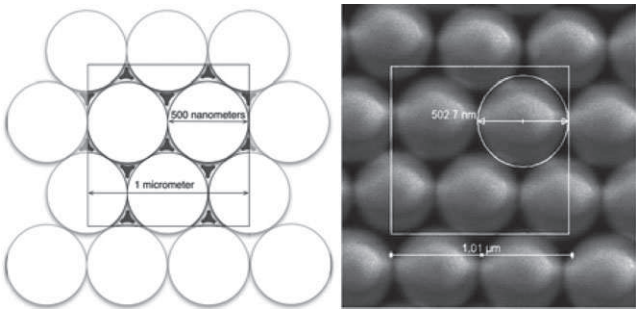

Figure 4 Left: scheme of the ideal nanowire density per square micrometer (10 wires per square micron), as allowed by geometrical factors in the hexagonal close packing of 500 nm spheres. Right: the corresponding SEM micrograph of the assembly.

For thermal evaporation, the metal grains are still separated even for higher thickness, while for high vacuum sputtered metal films the growth tends to be epitaxial and the metal clusters are more compact.

The density along the array is determined by the hcp configuration, as shown in Fig. 4, and verified in Fig. 5, with 500 nm spheres assembly, only 10 interstitial sites per a square unit cell of 1 μm are possible, extruding 10 wires during MAE.

In Fig. 3, the nanowire length and diameter distributions along the array are shown. This analysis has been carried out by using a shareware code for microscopy and morphological analysis, Image J, from NIH [29]. The diameter distribution appears to be a log-normal, typical of size dispersion in other nanostructured materials like porous silicon. The average is around 30 nm, and a possible data loss under 10 nm is possible due to SEM resolution and image processing tools, minimum pixel dimension limit.

The nanowire length distribution is not so trivial to be interpreted, showing a more complicate shape, with two different peaks around 300 and 40 nm. In particular, the last peak could be related to nanowire breaking or to an incomplete extrusion of the SiNW due to an unefficient removal of the silver layer by the sputter etching process. The small area of the shorter wires seems to indicate this possible reason. It must be remarked that the etching front is not completely homogeneous on the millimeter scale, and,

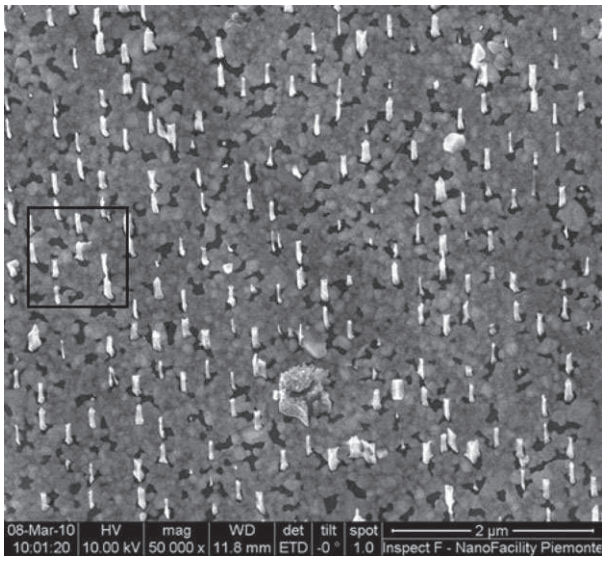

Figure 5 Closer view of the SiNWs. In this microphotograph the hcp arrangement due to the self-assembly of PSNS is evident. The black square on the left is one square micrometer, and the density of 10 SiNWs per 1 μm^2 is obtained, confirming the ideal scheme of Fig. 5.

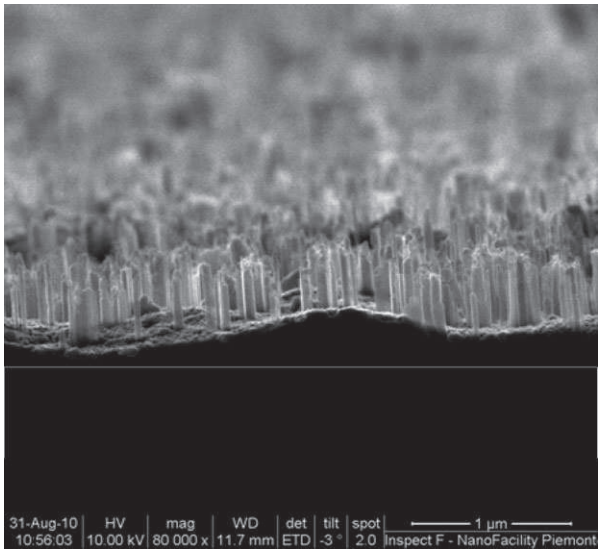

Figure 6 Cross section of the SiNWs array. A modulation in the etching front is clearly visible.

different heights of SiNWs are observed. This is probably due to the difficulty encountered by the etching solution to reach the interface between silver and silicon. Another aspect that could affect the homogeneity of the nanowire array is the hydrogen bubbling during silicon etching, affecting the array homogeneity on large scale. An additional effect is clearly visible in Fig. 6, as a sort of waviness in the etching front, also observed in porous silicon formation, and increasing with porous layer thickness. Work on different metals, like gold, and varying density and wettability of the etching solution, is in progress to ascertain this effect.

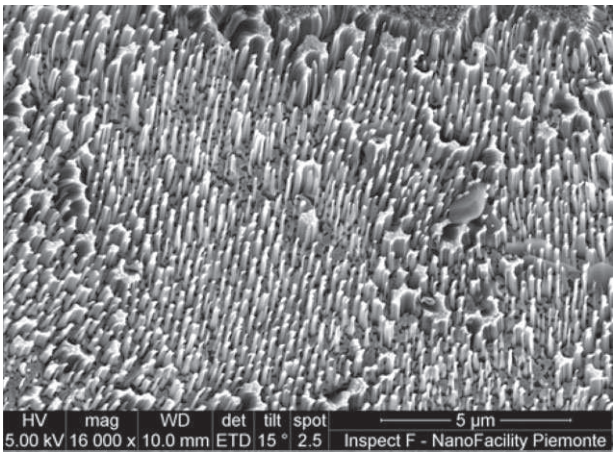

Figure 7 Ordered area of SiNWs as reported in Figs. 3 and 5, with longer etching times (60 s), resulting in longer SiNWs.

Despite the above described effects of the etching front modulation, the average extension of the areas where the morphological characteristics of the wires is rather large, this modulation affects mainly the length distribution over extensions of millimetres. The nanospheres self-assembly structure, influences only the order and the orientation of the wires, not the dimensions. The spheres in fact, tend to arrange in clusters of different orientation (see Fig. 7) of typical sizes ranging from few micrometers to 50–100 μm of side. These domains with single orientation are separated by linear defects. After MAE, these dislocations give origin to non-separate wires, so forming walls delimiting the domains. Inside the different domains the wires are rather homogeneous, in terms of diameter and length. The array orientation varies from zone to zone, exhibiting different 2D lattice orientation, reflecting the original disposition of the nanospheres.

The distance between nanowires is closely related to the sphere diameters, as expected, but under 100 nm the rapid etching rates are source of disorder. A dedicate and accurate choice of the etching parameters has still to be found. Work is in progress to get results on these small diameters.

Increasing etching times, longer wires have been obtained, as in Fig. 7, where a sample obtained by the same procedure of the previous is shown, but an etching time of 60 s has been used. For longer times of etching an erosion of the nanowire top has been observed due to pure chemical dissolution in HF, and collapsing and sticking among groups of wires is rather common, unless supercritical drying methods are used.

In conclusion, ordered arrays of SiNWs have been designed and fabricated with the combination of two techniques, self-assembly and MAE.

The simple variation of times during nanoindentation by sputter etching and during MAE, offers an easy and repeatable control of nanowires size and length, maintaining the order and the geometry introduced by nanospheres self-assembly.

Acknowledgements This work has been performed at NanoFacility Piemonte, INRiM, a laboratory supported by Compagnia di San Paolo.

References

[1] Y. Li, F. Qian, J. Xiang et al., Mater. Today **9**, 18 (2006).
[2] M. Menon, D. Srivastava, I. Ponomareva et al., Phys. Rev. B **70**, 12 (2004).
[3] T. Bozhi, X. Zheng, T. J. Kempa, Y. Fang, N. Yu, G. Yu, J. Huang, and C. M. Lieber, Nature **449**, 885 (2007).
[4] L. Qu, Y. Li, H. Zhang, Y. Huang, and X. Duan, Nano Lett. **9**, 4539 (2009).
[5] B. J. Alemn, K. E. Fischer, S. L. Tao, R. H. Daniels, E. M. Li, M. D. Bnger, G. Nagaraj, P. Singh, A. Zettl, and T. A. Desai, Nano Lett. **9**, 716 (2009).
[6] S. Chattopadhyay, Xiuling. Li, and P. W. Bohn, J. Appl. Phys. **91**, 6134 (2002).
[7] S. Bastide, C. Chartier, and C. Levy-Clement, Electrochim. Acta **53**, 5509 (2008).
[8] H. W. Deckman and J. H. Dunsmir, Appl. Phys. Lett. **41**, 377 (1982).
[9] M. Giersig and P. Mulvaney, Langmuir **9**, 3408 (1993).
[10] H. W. Deckman and J. H. Dunsmuir, Appl. Phys. Lett. **4**, 377 (1982).
[11] J. C. Hulteenand and R. P. Van Duyne, J. Vac. Sci. Technol. A **13**, 1553 (1995).
[12] M. Antonietti and K. Tauer, Macromol. Chem. Phys. **204**, 207 (2003).
[13] C. S. Chern, Prog. Polym. Sci. **31**, 443 (2006).
[14] C. Solans, P. Izquierdo, J. Nolla, N. Azemar, and M. J. Garcia-Celma, Curr. Opin. Colloid Interf. Sci. **10**, 102 (2005).
[15] J. M. Asua, Prog. Polym. Sci. **27**, 1283 (2002).
[16] C. A. Murray and D. H. V. Winkle, Phys. Rev. Lett. **58**, 1200 (1987).
[17] A. T. Skjeltorp and P. Meakin, Nature **335**, 424 (1988).
[18] N. D. Denkov, O. D. Velev, P. A. Kralchevsky, I. B. Ivanov, H. Yoshimura, and K. Nagayama, Nature **361**, 26 (1993).
[19] G. Picard, Langmuir **14**, 3710 (1998).
[20] A. J. Hurd and D. W. Schaefer, Phys. Rev. Lett. **54**, 1043 (1985).
[21] Z. Horvolgyi, M. Mate, and M. Zrinyi, Colloids Surf. A: Physicochem. Eng. Asp. **84**, 207 (1994).
[22] H. H. Wickman and J. N. Korley, Nature **393**, 445 (1998).
[23] X. Li and P. W. Bohn, Appl. Phys. Lett. **77**, 2572 (2000).
[24] H. Robbins and B. Schwartz, J. Electrochem. Soc. **123**, 1903 (1976).
[25] E. S. Kooij, K. Butter, and J. J. Kelly, Electrochem. Solid State Lett. **2**, 178 (1999).
[26] M. Winzer, M. Kleiber, N. Dix, and R. Wiesendanger, Appl. Phys. A **63**, 617 (1996).
[27] V. Lehmann, Electrochemistry of Silicon (WILEY-VCH Verlag GmbH, Weinheim, 2002), p. 58.
[28] B. Fuhrmann, H. S. Leipner, H. R. Höche, L. Schubert, P. Werner, and U. Gösele, Nano Lett. **5**, 2524 (2005).
[29] ImageJ, National Institutes of Health, USA. http://rsb.info.nih.gov/ij.

